Experimental observations of *s-p* coupling in copper dimer anions

Benkang Liu, Yanqiu Wang, and Li Wang*

State Key Laboratory of Molecular Reaction Dynamics, Dalian Institute of Chemical Physics, Chinese Academy of Science, Dalian, Liaoning 116023, People's Republic of China

(Received 17 June 2013; published 11 September 2013)

The photoelectron velocity-map image technique was employed to examine the one-photon detachment of Cu monomer and dimer anions using a linearly polarized infrared femtosecond laser. While the photoelectron angular distribution (PAD) in a single-photon detachment experiment of Cu^- shows no dependence on photon energy, the dimer anion PAD does show a strong dependence on photon energy. As the laser wavelength increases from 532 to 817 nm, the photoelectron angular distributions of the main one-photon detachment channel of the prominent detachment channel of Cu_2^- changes its direction from parallel to the direction of polarization for the 532-nm laser to perpendicular to the direction of polarization for the 817-nm laser. Based upon a numerical analysis of the anisotropy parameters, the relative contributions of the *s*, *p*, and *d* orbitals are obtained. The fully occupied *d* orbitals contribute less to the detachment amplitude. The contribution of the *p* waves to the detachment amplitude increases with the photon energy, while that of *s* waves decreases, which is in agreement with the prediction of the Wigner threshold law. The relative contributions of the different partial waves, *s* and *p*, to the detachment amplitude are altered by the excess energy of the detached electron, resulting in the determined shape of the photoelectron angular distributions. Our one-photon photodetachment experiments on the energy-dependent angular distributions of the copper anionic dimers indicate that *s-p* coupling is important to the photodetachment of copper dimer anions, especially at increased photon energies.

DOI: 10.1103/PhysRevA.88.033413 PACS number(s): 33.80.Eh, 32.80.Gc, 33.60.+q, 36.40.−c

I. INTRODUCTION

Recently, metal clusters have drawn considerable attention for their use in new applications and have led to a new field of cluster physics aimed at understanding how their properties arise and change with cluster size [1–3]. A jellium model (JM) had been proposed to account for the electronic shell structure of various metal clusters [4–7]. Although the model has been successfully applied to describe the ionization potentials in some metal clusters, such as Na_n [8] and Cu_n [9], in others, the ionization potentials have deviated significantly from the simple model [10–12]. For example, in Al_n clusters, the degree of *s-p* correlation changes dramatically and oscillates with cluster size. The largest *s-p* hybridization exists in Al_3^- anions, while the smallest hybridization exists in Al_4^- [12].

The introduction of a velocity-map imaging technique [13] led to increased interest in these methods for exploring the dynamics of photoionization and photodissociation of neutral species [14] and the photodetachment from negatively charged ions and clusters [12,15] in the gas phase. The integration of mass selectivity and photoelectron velocity mapping provides a valuable approach for investigating the size-dependent evolution of the electronic structure and dynamics of clusters [12,16]. The photoelectron angular distributions (PADs) carry the signature of the electronic structure of the anion, the neutral species, and the symmetry of the wave function for the detached electron [17,18], which may provide insight into the partial-wave composition of the molecular orbitals through which the detachment process occurs [12,19–21]. The PAD is characterized using an asymmetry parameter that is typically energy dependent [22]. The final-state interactions in the photodetachment process [23] can be understood through the energy dependence of the asymmetry parameter. PADs are typically well described by the single-electron model [23,24] in which the orbital angular momentum of the incoming photon is coupled only to the detaching electron neglecting all interactions involving the neutral core. Thus, emission from an *s* orbital yields a β value of $+2$, while emission from a *p* orbital (or higher orbital angular momentum state) results in two partial waves that can interfere to yield any β value between -1 and $+2$. However, electron correlations could be significant near the autoionization and autodetachment resonances and could induce a twist in the spectral dependency of the asymmetry parameters, as has been predicted theoretically [25] and observed experimentally near the autoionizing resonances of two-photon-excited iodine atoms [26]. Significant electron correlations in either the initial bound or final continuum state change the asymmetry parameter from that predicted by the single-electron model [27]. Electron correlations in the continuum state are called "channel coupling." Remarkable deviations in the asymmetry parameter can provide a convenient probe for autodetachment resonances. Experimental probing of such a deviation from the single-electron model is necessary in anions whose electronic structure and dynamics are largely determined by the electron correlations [28]. Recent photodetachment experiments of sodium cluster anions have indicated that PADs obtained using this method deviate strongly from the predictions of single-electron models, indicating that the correlated multielectron effects play a distinct role in the photoemission process [29].

In this work, a photoelectron imaging technique is used to probe the electronic structure of small copper anion clusters. Given their interesting electronic structures and promising applications in catalysis, optoelectronics, and nanophotonics, clusters of group IB elements (Cu, Ag, Au) have recently

*Corresponding author: liwangye@dicp.ac.cn

found particular interest. Early research suggested that the full d subshell makes little contribution to the electronic structure and geometry of the cluster (both anionic and neutral) as predicted theoretically [30,31]. Within the framework of the JM, the Cu 4s electrons are delocalized at the geometric boundaries of the cluster. Therefore, over the range of binding energies in which the density of states in the Cu clusters is dominated by the 4s derived states [32], the electronic structure should be similar to that of alkali metal clusters. The two main peaks in the photoelectron spectroscopy experiment (from the three outer-shell electrons in Cu_2^-) were assigned to the bonding σ and antibonding σ^* molecular orbitals of Cu_2 [28]. The symmetries of the molecular orbitals should be similar to the JM orbitals ($\sigma \leftrightarrow s$; $\sigma^* \leftrightarrow p$) [33]. Although some characteristics of these clusters are determined by their s valence electrons, the close proximity of the d orbitals significantly modifies their structural, electronic, and optical properties [27]. Copper clusters prove particularly challenging from a computational standpoint because the relevant atomic 3d wave functions are nodeless, making these valence orbitals highly localized. In addition, the s-d energetic separation is the smallest for Cu; the d electrons significantly alter various properties of the Cu clusters due to their strong hybridization with the sp electrons [27].

In a femtosecond one-photon detachment of the Cu anions, the PADs of the main detachment channel in Cu^- are independent of the laser wavelengths, as reported in the literature [28]. However, in the Cu_2^- systems, the PADs change significantly with the laser wavelength. The relative contributions of the s, p, and d orbitals are obtained by analyzing the anisotropy parameters. The relative contributions of the various partial waves to the detachment amplitude are altered by the excess energy in a detached electron, thus altering the shape of the PAD. Our report is an investigation of the energy-dependent angular distribution of copper dimer anions via femtosecond one-photon photodetachment.

II. EXPERIMENTAL SECTION

In the present study, the copper anions are formed from a laser vaporization metal cluster source in which the second-harmonic output (532 nm) of a neodymium-doped yttrium aluminum garnet laser (YAG laser, Quantel Brilliant) with a pulse duration of 5 ns operating at 20 Hz is focused on a rotating and translating copper rod to form a plasma. The metal plasma is then cooled using a helium carrier gas (99.9%) at a stagnation pressure of 0.4 MPa and is expanded into a vacuum through a pulsed valve (General Valve Corp.). As shown in Fig. 1, the central portion of the negative ions are extracted perpendicularly and accelerated into a McLaren-Wiley time-of-flight mass spectrometer using a -1.4-kV high-voltage pulse. Mass selection is achieved via three electrodes with a time-delayed, pulsed electric field applied to the central electrode. The mass-selected negative ions are then refocused onto the center of a time-delayed, pulsed velocity-mapping two-stage electric field and are photodetached using a time-delayed femtosecond laser pulse. The detached photoelectrons are accelerated and velocity focused toward a position-sensitive detector. After flying through a 40-cm field-free region, which is shielded against stray magnetic fields by a μ-metal tube, the photoelectrons are mapped onto a two-stage microchannel plate (MCP) detector backed by a phosphor screen. Images on the screen are captured using a thermoelectrically cooled charge-coupled device video camera (LaVision Inc., Imager QE). All photoelectron images are reconstructed using the PBASEX program [34,35], which can yield both the photoelectron energy spectra and the PADs [36,37].

In the presence of linearly polarized monochromatic fields, the expression for the angular-resolved differential one-photon detachment rate can be expanded as a function of the angle, θ, between the detection and laser field directions based on the Legendre polynomials [24]:

$$I(\theta) = I_0\{1 + \beta_2 P_2[\cos(\theta)]\}, \quad (1)$$

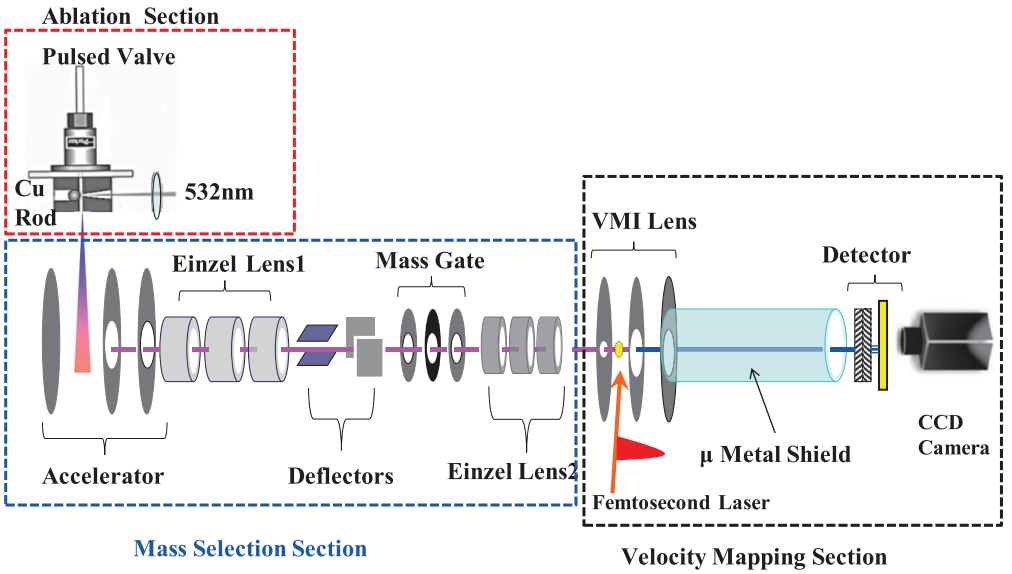

FIG. 1. (Color online) Schematic drawing of the experimental setup.

in which β_2 is the anisotropy parameter and $P_2(x) = (3x^2 - 1)/2$ is the Legendre polynomial.

Linearly polarized laser wavelengths of 532, 577, 586, 675, 708, and 736 nm are generated in a commercial optical parametric amplifier (Quantronix/Light Conversion, TOPAS) pumped by the fundamental output (centered at 817 nm with a 30-nm FWHM bandwidth and a 70-fs pulse width) of a solid-state femtosecond laser at a 20-Hz repetition rate with 10 mJ/pulse. The laser pulse width is determined via single-shot intensity autocorrelation. The laser pulses at 408 nm are the second-harmonic generation of the fundamental output (817 nm) with a thin type-1 BBO crystal. The pulse energies at these wavelengths are maintained at approximately 200 μJ in the interaction region. The laser beam is focused with a 50-cm focal-length lens with a polarization direction parallel to the detector plane. The focus size is measured using the pinhole method. The laser intensity in the interaction region is carefully controlled to prevent multiphoton detachment.

III. RESULTS AND DISCUSSION

The raw photoelectron images obtained from the single-photon detachment of the Cu^- anions by the 577 nm (2.15 eV) and 408 nm (3.04 eV) femtosecond laser (a) and (e), the corresponding reconstructed images (b) and (f), the photoelectron spectra (c) and (g) and the PADs of the outermost rings in the images (d) and (h) are summarized in Fig. 2. The prominent peaks of Cu^- in Figs. 2(c) and 2(g) are assigned to the removal of an electron from the fully occupied 4s orbital of the anion to the ground state of the neutral atom, which corresponds to the (Cu $3d^{10}4s^1\,^2S_{1/2} \leftarrow Cu^-$ $3d^{10}4s^2\,^1S_0$) transition. This peak is centered at an electron binding energy of 1.24 ± 0.06 eV. Considering the energy width of a femtosecond laser (approximately 0.06 eV at 817 nm, for example), the binding energy of 1.24 ± 0.06 eV obtained in our single-photon detachment experiment is close to the value of 1.235 ± 0.005 eV obtained using a narrow bandwidth nanosecond laser [38,39].

The outgoing electron in the single-photon detachment of Cu^- ($3d^{10}4s^2\,^1S_0$) can be described using a pure p-wave function. The anisotropy parameters of the photoelectron image at these two wavelengths, β_2, as shown in Figs. 2(d) and 2(h), are approximately 1.97 ± 0.03 and 2.04 ± 0.04, respectively, which match that in Sobhy's experiment (2.0 ± 0.06) at 400 nm [21] and that in Aravind's experiment (1.94 ± 0.05) at 532 nm [28]. The other two inner rings in the images in Figs. 2(e) and 2(f) and the corresponding peaks at higher binding energies in Fig. 2(g) are due to the spin-orbit coupled transitions, Cu $3d^9 4s^2\,^2D_{3/2} \leftarrow Cu^-$ $3d^{10}4s^2\,^1S_0$ with a binding energy of 2.62 ± 0.02 eV [39] and Cu $3d^9 4s^2\,^2D^{5/2} \leftarrow Cu^-$ $3d^{10}4s^2\,^1S_0$ with a binding energy of 2.88 ± 0.02 eV [39]. These results are in good agreement with those of previous reports. The two ^2D transitions result from the detachment of a 3d electron and produce partial p and f wave functions with an anisotropy parameter value near zero.

Aravind *et al.* [28] attempted to verify the influence of electron correlations on the absolute photodetachment cross section for Cu^- for photon energies above 3.5 eV predicted by theoretical calculations [38]. No significant influence from the channel-coupling effect on the PAD was found experimentally in the photon energy range of 3.46–4.6 eV [28]. Our experimental observations, as shown in Fig. 2, also suggest a lack of evidence for the influence of electron correlations on the absolute photodetachment cross section for Cu^-.

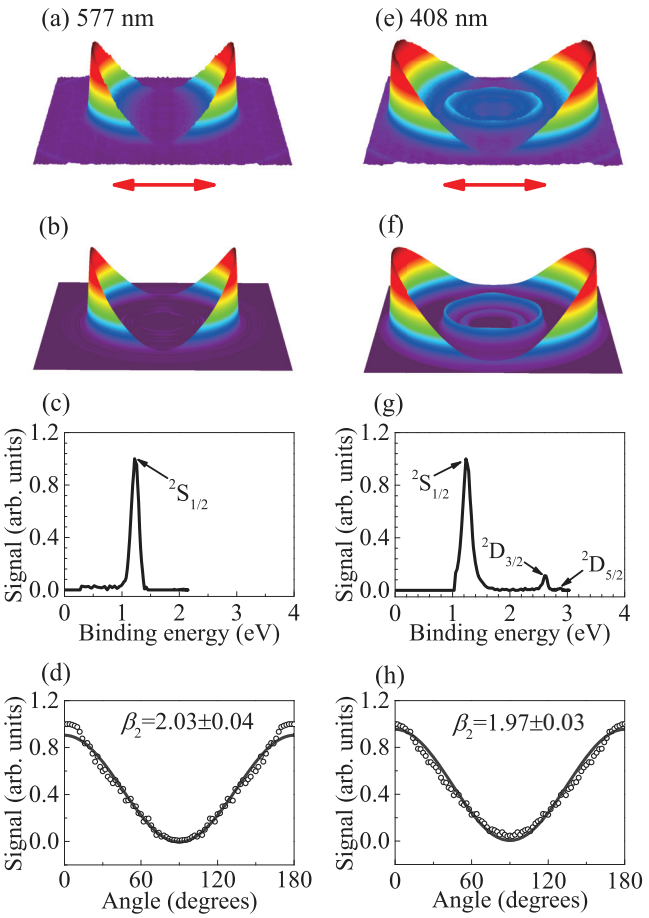

FIG. 2. (Color online) One-photon detachment results for Cu^- at 577 nm (left column) and 408 nm (right column). Raw photoelectron images (a) and (e), inverse images (b) and (f), photoelectron kinetic energy spectra (c) and (g), and angular distributions of the main detachment channel (d) and (h). Double arrow lines in (a) and (e) represent the direction of the laser polarization. Solid lines in (d) and (h) are the best fitting results of the PAD to the expression $I(\theta) = I_0\{1 + \beta_2 P_2[\cos(\theta)]\}$ in the angle range from 5° to 175°.

In the case of Cu dimer anions, the photodetachment process changes dramatically with the laser wavelengths, differing completely from that of the Cu monomer anions as illustrated in Fig. 3. The PADs of the prominent detachment channel at a laser wavelength of 817 nm are perpendicular to the direction of laser polarization, while at 532 nm, the angular distributions are parallel. The corresponding anisotropy parameters of the photoelectron image at these wavelengths are illustrated in Fig. 4(a).

Due to the intrinsically broad energy resolution of femtosecond lasers (approximately 0.06 eV at 817 nm), the vibrational resolution in a femtosecond photodetachment of the Cu dimer anion is unachievable. According to the results of previous high-resolution photoelectron energy spectra, the energy gap between the 0-0 and 0-1 transition is approximately

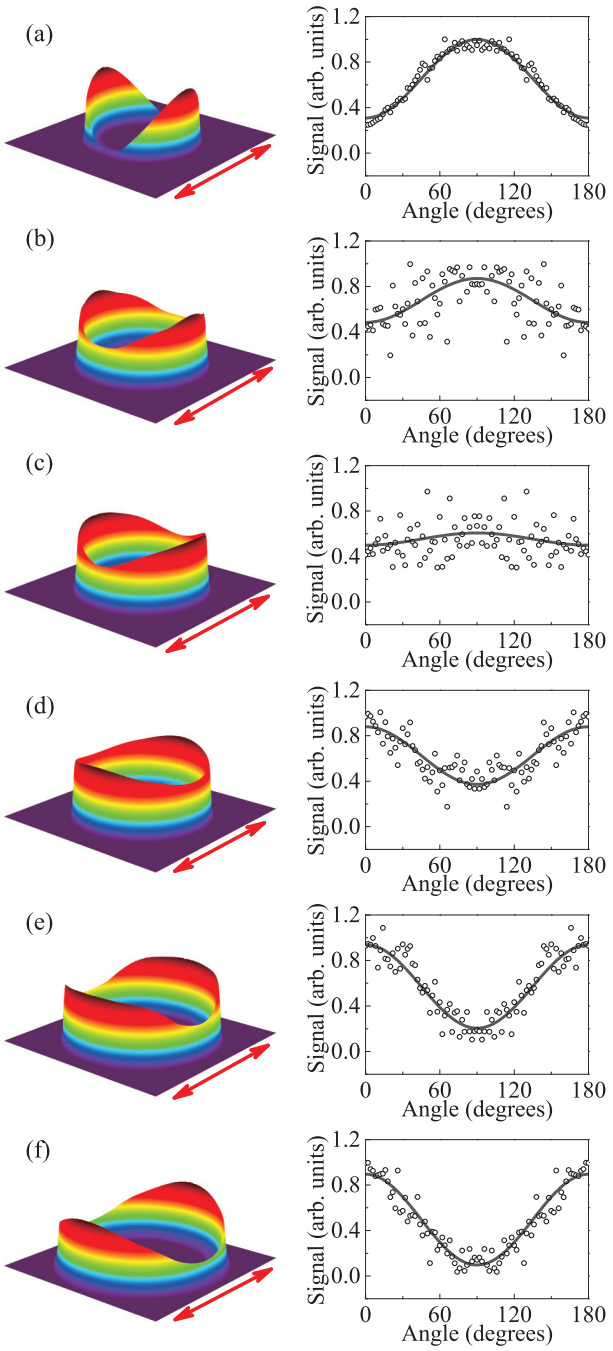

FIG. 3. (Color online) One-photon detachment results for Cu_2^- at (a) 817, (b) 736, (c) 708, (d) 675, (e) 586, and (f) 532 nm. Left column: inverse images; right column: corresponding angular distributions of the main detachment channel. Double arrow lines in left column represent the direction of the laser polarization. Solid lines in right column are the best fitting results of the PAD to the expression $I(\theta) = I_0\{1 + \beta_2 P_2[\cos(\theta)]\}$ in the angle range from 5° to 175°.

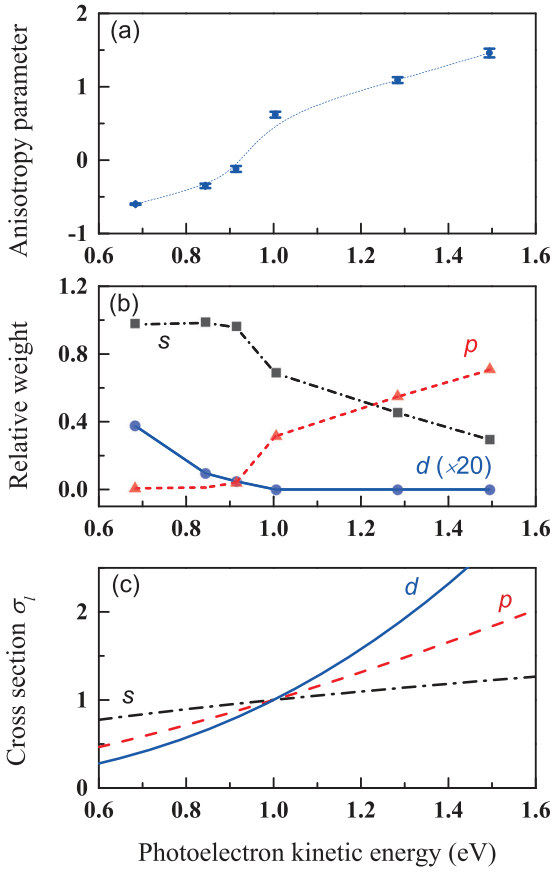

FIG. 4. (Color online) Excess energy-dependent anisotropy parameters of the principal one-photon detachment channel of Cu_2^-. (a) Anisotropy parameters, (b) relative contributions of the s, p, and d characters, (c) detachment cross-sectional predictions of s, p, and d using the Wigner threshold law.

266 cm^{-1} (0.03 eV). The dominant detachment channel is due to the transition of the Cu_2^- ground state $X\,^2\Sigma_u^+$ ($\sigma_g^2\,\sigma_u^{*1}$, $\upsilon' = 0$) to the Cu_2 ground state $X\,^1\Sigma_g^+$ (σ_g^2, $\upsilon' = 0$) [39]. According to the simple molecular orbital theory (MO), the two s atomic orbitals (AOs) of Cu form a bonding σ_g MO and an antibonding σ_u^* MO. The resulting electronic states and configurations are Cu_2^- $X\,^2\Sigma_u^+$ ($\sigma_g^2\,\sigma_u^{*1}$) and Cu_2 $X\,^1\sigma_g^+$ (σ_g^2). Based upon the simple MO model, the formal bond order should be one half for the Cu_2^- ground state and one for the Cu_2 singlet ground state. Thus, one might expect Cu_2^- to have a smaller dissociation energy than the ground Cu_2 singlet state. However, the anion bond energy of Cu_2^- is estimated to be 1.62 ± 0.20 eV [39], which is more than 80% of the neutral singlet bond energies of 2.02 ± 0.08 eV [39]. This result indicates that the simple ns orbital bonding picture does not adequately reflect the bond strengths for the diatomic molecules of the transition metals. The contributions of the $3d$ and $4p$ orbitals to the Σ_u MOs must also be considered. For copper, the $3d$ shell is fully occupied and thus has little direct influence on bonding, but the $4p$ orbitals are available and have energies near those of the $4s$ orbitals [40]. According to the *ab initio* calculations [41], the $4s$ σ_u^* orbital should be extensively polarized in the dimer systems of Cu_2 and Cu_2^- through the mixing of $4p$ orbitals. This polarization decreases the electron density between the two nuclei, reducing the antibonding character of the $4s$ σ_u^* and resulting in an anion bond energy that is nearly as strong as the $(4s\sigma_g)^2$ neutral singlet [41]. The theoretical calculations indicate that the d-d correlation and relativistic effects in the Cu neutral and anionic dimers are relatively small, while the core s-p correlation is

significantly more important to the spectroscopic constants of Cu_2 [42].

Considering the possible contribution of the p orbital to the emitting photoelectron in the detachment of Cu_2^-, the detached electrons may have an angular momentum of 0 or 2 ($l \pm 1$, l is the orbital angular momentum of the detached electron), i.e., the s and d waves should be mixed in the final state. Reichle *et al*. [43] presented an approach to extract the complex partial-wave amplitudes of the final continuum state as a function of the electron energy. The PADs are fitted to the partial-wave decomposition of the n-photon detachment rate as follows [43]:

$$I(\theta) \propto \left| \sum_{L=0}^{L_{\max}} f_L^{(n)} Y_{L0}(\theta,\phi) \right|^2 , \tag{2}$$

in which L denotes the angular momentum of the outgoing electron and Y_{L0} represents the corresponding spherical harmonic. As in the case of an ideal linear polarization and isotropic initial state, only terms with zero projection of the angular momentum contribute to the sum. The complex amplitudes $f_L^{(n)}$ are determined in the fit. The parity of the final state is defined by the number n of absorbed photons, and either an odd or even L contributes to the sum in Eq. (2). The number of fitting parameters is $L_{\max}$ or $L_{\max} \pm 1$ for the odd or even final-state parity, respectively. For photodetachment from a superposition of s and p states, the angular dependence may be expanded as a linear combination of one s- and one p-type function [44]; the one-electron model from such an s-p mixed stationary state can be expressed as follows:

$$|\psi_i\rangle = f_s\,|s\rangle + \sqrt{1 - f_s^2}\,|p\rangle\,, \tag{3}$$

in which f_s is the fractional s character of the $|\psi_i\rangle$ state ($0 \leqslant f_s \leqslant 1$). Any relative phase factors for the s and p contributions to the $|\psi_i\rangle$ state are absorbed into the corresponding kets. From a pure s state, the final accessible one-photon detachment state is a p state, which has a wave function that can be expressed as $\sqrt{3/2}P_1(\cos\theta)$, in which the factor $\sqrt{3/2}$ is added as normalization coefficient. From a pure p state, a mixed state ψ_j of s and d orbitals can be reached from a one-photon absorption as described by Eq. (4).

$$|\psi_j\rangle = (|s\rangle + f_d|d\rangle)/\sqrt{1 + f_d^2}, \tag{4}$$

in which f_d is the fractional d character of the $|\psi_j\rangle$ state ($0 \leqslant f_d \leqslant 1$). The factor $\sqrt{1 + f_d^2}$ is added as a normalization coefficient.

Substituting Eqs. (3) and (4) into Eq. (2) yields Eq. (5):

$$I(\theta) \propto \left(1 - f_s^2\right) \left| \frac{(|s\rangle + f_d|d\rangle)}{\sqrt{1 + f_d^2}} \right|^2 + \left| f_s \sqrt{\frac{3}{2}} P_1(\cos\theta) \right|^2 . \tag{5}$$

By fitting experimental results with Eq. (5), one can obtain the relative contributions of s, p, and d components, which are expressed by the formulas $(1 - f_s^2)/(1 + f_d^2)$, f_s^2, and $(1 - f_s^2)f_d^2/(1 + f_d^2)$, respectively. The relative contributions of the s, p, and d waves at different laser wavelengths are illustrated in Fig. 4(b). The contribution of the d partial wave is much smaller than those of the s and p waves.

Previous research determined that the detachment process near the negative ion threshold follows the Wigner threshold law [45–48]. Near the detachment threshold, the photodetachment cross section has the form $\sigma_L \propto E^{L+1/2}$, in which L is the angular momentum of the outgoing electron and E is the excess energy. The short-range final-state interactions can affect the range of the validity of the Wigner law, but do not alter its form [46]. As mentioned in Refs. [12] and [47], near the detachment threshold, partial waves with less orbital angular momentum such as the s wave dominate the photodetachment amplitude. As the excess energy increases, the contribution of the p and d wave components to the detachment signal becomes prominent. When the excess photoelectron energy exceeds more than tens of meV above threshold, the Wigner law typically begins to fail [47]. There were also some exceptions [46,48]. In the case of Cl^-, the detachment cross section also followed the Wigner law with electron energy around 0.125 eV [46]. For inner-shell electron detachment of He^- and S^-, Bilodeau *et al*. [48] found the cross section behaviors for both s and p components were surprisingly consistent with the Wigner threshold law with the excess energy more than an order of magnitude greater than the range found in valence photodetachment. For s-wave detachment, the Wigner law was found to be valid up to 3 eV kinetic energy above threshold, and the d-wave channel gave even better agreement over this energy range [48]. This unprecedented range of validity for the Wigner law was inconsistent with standard threshold law corrections [47] and has remained difficult to explain up to date.

The photodetachment of anions near the detachment threshold has drawn attention because, in this energy range, the electron-correlation effects and interferences become more prominent. As suggested in Ref. [12], this threshold law is not a strict relationship that can be quantitatively employed in the higher excess energy range, but may provide qualitative insight of how the relative weights of the partial waves vary with the photoelectron kinetic energy. However, comparison between threshold law prediction and experimental results may provide indirect evidence for the existence of an s-p correlation in the detachment of the Cu dimer anions. The detachment cross-sectional predictions of s, p, and d using the Wigner threshold law are illustrated in Fig. 4(c). The relative contribution of the p wave increases with the excess energy, while that of the s component decreases. In a metal cluster anion system, the range of validity of the law, to the best of our knowledge, has not been well addressed up to date.

One obvious phenomenon depicted in Fig. 4 is that, in the range of photoelectron kinetic energy near 1 eV, the anisotropy parameters (a), relative contributions of s, p, and d character (b), and detachment cross-sectional predictions of s, p, and d using the Wigner threshold law (c) change dramatically. The aforementioned contribution from the fully occupied closed d shell to the detachment is believed to be small, as illustrated in Fig. 4(b). Comparison between Figs. 4(b) and 4(c) shows that the Wigner threshold law provides qualitative insight into the photodetachment process for copper dimer anions over a substantial excess energy range, in our experiment, up to 1.6 eV. This is, to some extent, similar to the inner-shell electron detachment of atomic anions [48].

The above arguments also apply to Ag dimer anions because both the electronic configuration and the structure of the Ag_2^- are similar to those of the Cu dimer anions. Similar phenomena should be observed in the photodetachment of Ag_2^-. In fact, preliminary results of experiments we have conducted indicate that the PADs of the main detachment of Ag_2^- also change significantly with the laser wavelength.

IV. CONCLUSION

We report the one-photon detachment of the Cu monomer and dimer anion using a linearly polarized infrared femtosecond laser. Photoelectron velocity-map imaging technique was employed to examine the photoelectron angular distributions (PADs). While the PAD in a single-photon detachment experiment of Cu^- shows no dependence on photon energy, the dimer anion PAD does show a strong dependence on photon energy. As the laser wavelength increases from 532 to 817 nm, the PADs of the prominent detachment channel change from parallel to the direction of polarization for the 532-nm laser pulses to perpendicular to the direction of polarization for the 817-nm laser pulses, indicating that a simple molecular orbital picture could not fully describe the electronic structure of the Cu dimer anions. The contributions of the d and p orbitals to the photodetachment process should also be considered. Based on a numerical analysis of the anisotropy parameters, the relative contributions of the s, p, and d partial waves are obtained. The fully occupied d orbitals have a smaller contribution to the detachment amplitude. The contribution of the p waves to the detachment amplitude increases with photon energy, while that of the s waves decreases. In the range of photoelectron kinetic energies near 1 eV, the relative contributions of the s and p character change significantly, which is in good agreement with the prediction of the Wigner threshold law. The relative contributions of the various partial waves (s and p) to the detachment amplitude are altered by the excess energy of the detached electron, and as a result, alter the shape of the PAD. We report here on the energy-dependent angular distributions of copper dimer anions using femtosecond, one-photon photodetachment. Our experiments indicate that s-p coupling plays an important role in the photodetachment of copper dimer anions, especially at increased photon energy.

ACKNOWLEDGMENTS

The authors gratefully acknowledge support by the National Natural Science Foundation of China (Grants No. 21073188 and No. 21303199) and the National Major Scientific Instruments and Equipments Special Project of China (Grant No. 2011YQ05006903).

[1] D. E. Bergeron, P. J. Roach, A. W. Castleman, Jr., N. O. Jones, and S. N. Khanna, Science **307**, 231 (2005).
[2] J. U. Reveles, S. N. Khanna, P. J. Roach, and A. W. Castleman, Jr., Proc. Natl. Acad. Sci. USA **103**, 18405 (2006).
[3] A. W. Castleman, Jr. and S. N. Khanna, J. Phys. Chem. C **113**, 2664 (2009).
[4] M. Brack, Rev. Mod. Phys. **65**, 677 (1993).
[5] M. Itoh, V. Kumar, T. Adschiri, and Y. Kawazoe, J. Chem. Phys. **131**, 174510 (2009).
[6] W. A. de Heer, Rev. Mod. Phys. **65**, 611 (1993).
[7] A. Kaufmann, A. Kornath, A. Zoermer, and R. Ludwig, Inorg. Chem. **49**, 3851 (2010).
[8] W. D. Knight, K. Clemenger, W. A. de Heer, W. A. Saunders, M. Y. Chou, and M. L. Cohen, Phys. Rev. Lett. **52**, 2141 (1984).
[9] M. B. Knickelbein, Chem. Phys. Lett. **192**, 129 (1992).
[10] W. A. de Heer, P. Milani, and A. Châtelain, Phys. Rev. Lett. **63**, 2834 (1989).
[11] C.-Y. Cha, G. Gantefor, and W. J. Eberhardt, J. Chem. Phys. **100**, 995 (1994).
[12] J. J. Melko and A. W. Castleman, Jr., Phys. Chem. Chem. Phys. **15**, 3173 (2013).
[13] A. T. J. B. Eppink and D. H. Parker, Rev. Sci. Instrum. **68**, 3477 (1997).
[14] L. Wang, H. Kohguchi, and T. Suzuki, Faraday Discuss. **113**, 37 (1999).
[15] E. Surber and A. Sanov, J. Chem. Phys. **116**, 5921 (2002).
[16] R. Mabbs, E. Surber, L. Velarde, and A. Sanov, J. Chem. Phys. **120**, 5148 (2004).
[17] K. J. Reed, A. H. Zimmerman, H. C. Andersen, and J. I. Brauman, J. Chem. Phys. **64**, 1368 (1976).
[18] M. S. Bowen and R. E. Continetti, J. Phys. Chem. A **108**, 7827 (2004).
[19] E. Surber, R. Mabbs, T. Habteyes, and A. Sanov, J. Phys. Chem. A **109**, 4452 (2005).
[20] S. M. Bellm and K. L. Reid, Chem. Phys. Lett. **395**, 253 (2004).
[21] M. A. Sobhy and A. W. Castleman, Jr., J. Chem. Phys. **126**, 154314 (2007).
[22] S. T. Manson and A. F. Starace, Rev. Mod. Phys. **54**, 389 (1982).
[23] G. Aravind, A. K. Gupta, M. Krishnamurthy, and E. Krishnakumar, Phys. Rev. A **76**, 042714 (2007).
[24] J. Cooper and R. N. Zare, J. Chem. Phys. **48**, 942 (1968).
[25] A. N. Grum-Grzhimailo, S. Fritzsche, P. O'Keeffe, and M. Meyer, J. Phys. B **38**, 2545 (2005).
[26] S. Tauro and K. P. Liu, J. Phys. B **41**, 225001 (2008).
[27] K. Baishya, J. C. Idrobo, S. Öğüt, M. Yang, K. A. Jackson, and J. Jellinek, Phys. Rev. B **83**, 245402 (2011).
[28] G. Aravind, N. Bhargava Ram, A. K. Gupta, and E. Krishnakumar, Phys. Rev. A **79**, 043411 (2009).
[29] C. Bartels, C. Hock, J. Huwer, R. Kuhnen, J. Schwöbel, and B. von Issendorff, Science **323**, 1323 (2009).
[30] C. W. Bauschlicher, Jr., S. R. Langhoff, and P. R. Taylor, J. Chem. Phys. **88**, 1041 (1988).
[31] R. Pou-Amérigo, M. Merchán, I. Nebot-Gil, P. Å. Malmqvist, and B. O. Roos, J. Chem. Phys. **101**, 4893 (1994).
[32] O. Cheshnovsky, K. J. Taylor, J. Conceicao, and R. E. Smalley, Phys. Rev. Lett. **64**, 1785 (1990).
[33] C.-Y. Cha, G. Ganteför, and W. Eberhardt, J. Chem. Phys. **99**, 6308 (1993).
[34] G. A. Garcia, L. Nahon, and I. Powis, Rev. Sci. Instrum. **75**, 4989 (2004).

[35] P. O'Keeffe, P. Bolognesi, M. Coreno, A. Moise, R. Richter, G. Cautero, L. Stebel, R. Sergo, L. Pravica, Y. Ovcharenko, and L. Avaldi, Rev. Sci. Instrum. **82**, 033109 (2011).
[36] B. K. Liu, Y. Q. Wang, and L. Wang, J. Phys. Chem. A **116**, 118 (2012).
[37] R. C. Bilodeau, M. Sheer, and H. K. Haugen, J. Phys. B **31**, 3885 (1998).
[38] K. F. Scheibner and A. U. Hazi, Phys. Rev. A **38**, 539 (1988).
[39] J. Ho, K. M. Ervin, and W. C. Lineberger, J. Chem. Phys. **93**, 6987 (1990).
[40] C. E. Moore, *Atomic Energy Levels*, Natl. Stand. Ref. Data Ser., Natl. Bur. Stand. (US) (US GPO, Washington, DC, 1971).
[41] T. H. Upton, J. Chem. Phys. **86**, 7054 (1987).
[42] M. F. Jarrold, J. E. Bower, and J. S. Kraus, J. Chem. Phys. **86**, 3876 (1987).
[43] R. Reichle, H. Helm, and I. Yu. Kiyan, Phys. Rev. A **68**, 063404 (2003).
[44] E. R. Grumbling and A. Sanov, J. Chem. Phys. **135**, 164302 (2011).
[45] E. P. Wigner, Phys. Rev. **73**, 1002 (1948).
[46] R. Trainham, G. D. Fletcher, and D. J. Larson, J. Phys. B **20**, L777 (1987).
[47] J. W. Farley, Phys. Rev. A **40**, 6286 (1989).
[48] R. C. Bilodeau, J. D. Bozek, N. D. Gibson, C. W. Walter, G. D. Ackerman, I. Dumitriu, and N. Berrah, Phys. Rev. Lett. **95**, 083001 (2005).